

# A sensitivity assessment of millimeter-wave polarimetry for measurement of magnetic fluctuations associated with microtearing modes in NSTX-U

J Zhang<sup>1</sup>, N A Crocker<sup>1</sup>, W A Peebles<sup>1</sup>, T A Carter<sup>1</sup> and W Guttenfelder<sup>2</sup>

<sup>1</sup> Department of Physics and Astronomy, UCLA, Los Angeles, CA 90095-7099, USA

<sup>2</sup> Princeton Plasma Physics Laboratory, Princeton, NJ 08543-0451, USA

E-mail: [xyzhangj@physics.ucla.edu](mailto:xyzhangj@physics.ucla.edu)

Received 21 November 2012, in final form 11 January 2013

Published 15 March 2013

Online at [stacks.iop.org/PPCF/55/045011](http://stacks.iop.org/PPCF/55/045011)

## Abstract

Recent nonlinear gyrokinetic calculations have indicated that microtearing modes are driven unstable in NSTX (National Spherical Torus experiment) and may account for the observed anomalous electron thermal transport (Guttenfelder *et al* 2011 *Phys. Rev. Lett.* **106** 155004). In order to study magnetic fluctuations of both coherent and incoherent modes, a 288 GHz ( $\lambda \approx 1$  mm) polarimeter is under development (Zhang *et al* 2012 *Rev. Sci. Instrum.* **83** 10E321) for NSTX-U (NSTX-Upgrade) (Menard *et al* 2012 *Nucl. Fusion* **52** 083015). The system will utilize a retro-reflective geometry and view the plasma along the major radius close to the midplane. In order to assess whether the system will have sufficient sensitivity to observe microtearing modes in NSTX-U, a synthetic diagnostic code is developed and utilized to determine the expected phase fluctuation level. The fluctuating profiles for density and magnetic field generated by the non-linear gyrokinetic simulation are used as input to the code. Results indicate that the polarimeter phase fluctuation level due to the modeled microtearing modes is  $\gtrsim 2^\circ$ . Utilizing the same model, it was also established that the calculated phase fluctuations are dominated by magnetic, not density fluctuations. This was especially true when the horizontal viewing chord was close (within  $\pm 5$  cm) to the plasma midplane. These results indicate that the polarimeter planned for NSTX-U should have sufficient sensitivity to observe magnetic fluctuations associated with microtearing modes.

(Some figures may appear in colour only in the online journal)

## 1. Introduction

Polarimetry measures the electromagnetic wave polarization changes that result from propagation through a magnetized plasma. The diagnostic is a powerful technique to probe internal magnetic fields in magnetically confined plasmas, especially field fluctuations [4–8]. However, to date, there has been no study to investigate the possibility of employing this diagnostic to measure magnetic fluctuations associated with microtearing modes [1, 9]. A 288 GHz polarimeter has been under development [2] for the National Spherical Torus experiment-Upgrade (NSTX-U) [3] that will facilitate

investigation of microtearing modes. Microtearing modes are small scale tearing modes with large toroidal ( $n$ ) and poloidal ( $m$ ) mode numbers that have been predicted to be unstable in STs [10–12]. They are also predicted to be a significant contributor to anomalous electron thermal transport in some neutral beam heated ST plasmas. Theoretically they are driven unstable by having an electron-temperature gradient  $\nabla T_e$  projected onto helically resonant radial perturbations of magnetic field lines,  $\delta B_{mn}$ , with a rational value of the safety factor,  $q = m/n$ . The parallel component of  $\nabla T_e$  can drive a resonant parallel current, which reinforces  $\delta B_{mn}$  via Ampère's law [1]. The induced magnetic islands overlap

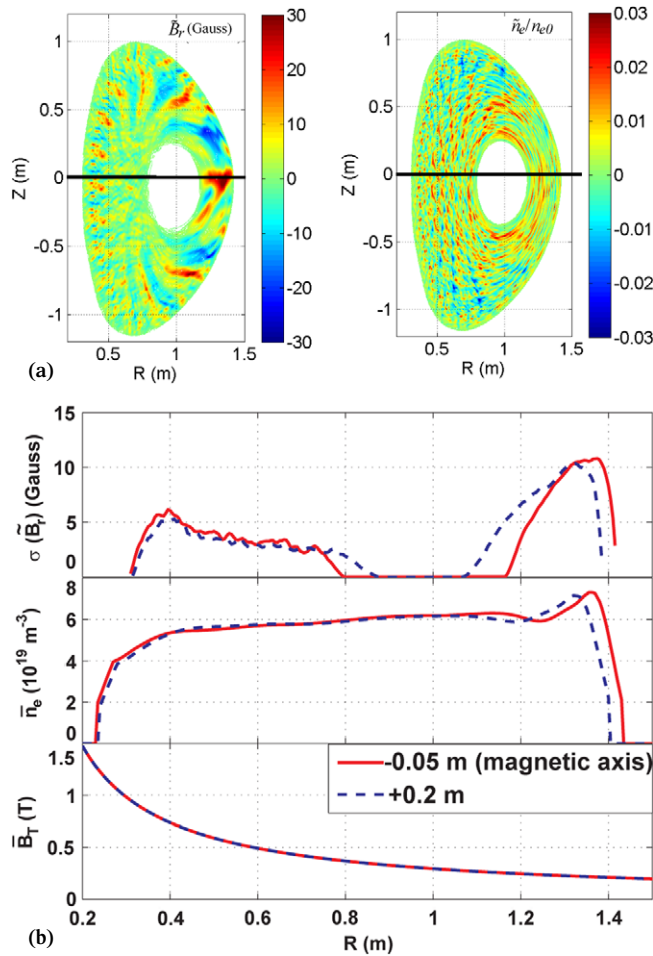


**Figure 1.** (a) A snapshot of radial magnetic fluctuations ( $\tilde{B}_r$ ) and normalized density fluctuations ( $\tilde{n}_e/n_{e0}$ ) associated with microtearing modes in an  $(R, Z)$  toroidal plane on NSTX generated by nonlinear gyrokinetic simulations. These islands rotate poloidally as time evolves. The horizontal lines indicate the horizontal beam path of the planned 288 GHz polarimeter.

(b) shows the radial profiles of standard deviation of  $\tilde{B}_r$  ( $\sigma(\tilde{B}_r)$ ), equilibrium electron density ( $\bar{n}_e$ ) and toroidal field ( $\bar{B}_T$ ) along the chords 0.05 below (solid line) and 0.2 m above (dashed line) machine midplane, respectively. Note that the two curves almost overlay in the third panel.

adjacent rational surfaces, leading to stochasticity. Electrons can then free-stream along the perturbed field line trajectories, which occurs more easily in the presence of many high- $n$  toroidal modes, thereby enhancing transport. The first successful non-linear gyrokinetic simulations have recently been reported for parameters based on an NSTX discharge (shot #120968, time = 0.560 s,  $B_T = 0.35$  T,  $I_p = 0.7$  MA,  $R/a = 0.82$  m/0.62 m,  $P_{\text{NBI}} = 4$  MW, line-averaged electron density  $n_e = 5.4 \times 10^{19} \text{ m}^{-3}$ ) that is unstable to only microtearing modes [1, 13]. Figure 1 shows a snapshot of the radial magnetic fluctuations ( $\tilde{B}_r$ , normal to flux surfaces), and normalized electron density fluctuations ( $\tilde{n}_e/n_{e0}$ ) associated with the microtearing modes in an  $(R, Z)$  toroidal plane on NSTX, as well as the radial profiles of  $\tilde{B}_r$  standard deviation, equilibrium density and toroidal field along the chords across ( $-0.05$  m) and above ( $+0.2$  m) the magnetic axis. As can be seen from figure 1(a), in the outboard region, the magnetic

fluctuations are spatially broad and strong (amplitude  $\sim 30$  G,  $\sim 1\%$  of local equilibrium field), while in the inboard region, they are finer in structure and relatively weaker. In contrast, the density fluctuations in the outboard region are poloidally elongated ( $k_\theta \rho_s \approx 0.2$ ,  $\rho_s = c_s/\Omega_i$ ,  $c_s = \sqrt{T_e/m_i}$ ,  $\Omega_i = Z_i e B/m_i$ ) but radially narrow ( $k_r \rho_s \gg 0$ ) with the fluctuation strength being roughly uniform (amplitude  $\sim 2\%$  of local equilibrium density). The proposed 288 GHz polarimeter complements other diagnostics planned for NSTX-U that might also be applied to the investigation of microtearing modes. The beam emission spectroscopy (BES) diagnostic planned for NSTX-U will probe density fluctuations, but the small radial scales that characterize microtearing mode density fluctuations pose a challenge for BES. The upgraded high- $k$  scattering diagnostic planned for NSTX-U potentially has the required sensitivity to probe microtearing mode density fluctuations [13]. In contrast, the polarimeter can potentially be employed to directly probe microtearing mode magnetic fluctuations without being adversely affected by the small scale density fluctuations. In figure 1(a) the solid horizontal lines indicate the retro-reflecting diagnostic viewing chord of the polarimeter, which lies along a major radius near the plasma midplane. The sensitivity of the polarimeter to microtearing modes is investigated in detail using a recently developed synthetic diagnostic code [14], which calculates the polarimeter response to given input density and magnetic profiles from the previously mentioned nonlinear gyrokinetic simulation [13]. The calculations indicate that the polarimeter phase fluctuation response due to the microtearing modes is  $\gtrsim 2^\circ$ . They also demonstrate that the phase fluctuations are dominated by the magnetic, not density fluctuations. This is especially true when the horizontal viewing chord is close (within  $\pm 5$  cm) to the plasma midplane.

This paper is presented in the following order: section 2 briefly describes the proposed polarimeter system and the algorithm of the synthetic diagnostic code; in section 3, results of the synthetic diagnostic calculations for microtearing modes are shown and discussed; conclusions are given in section 4; the appendix briefly reviews the major steps of the Mueller-Stokes analysis employed in this work.

## 2. The 288 GHz polarimeter system and synthetic diagnostic code

A schematic of the polarimeter system is shown in figure 2. More detailed description of the system hardware can be found in [2]. A rotating linearly polarized beam is launched along a major radius into NSTX plasma from the outboard side. The beam retro-reflects from a flat reflective graphite tile on the center stack, propagates through the plasma a second time, and returns to a polarization sensitive detector, which is aligned to detect the beam  $E$ -field component in the toroidal direction and outputs a sinusoidal waveform. Another reference sinusoidal waveform synchronized with the polarization rotation is generated in the process of producing the millimeter waves. By comparing the phase of these two waveforms, the polarization changes due to the magnetized plasma can be determined. For example, pure Faraday rotation

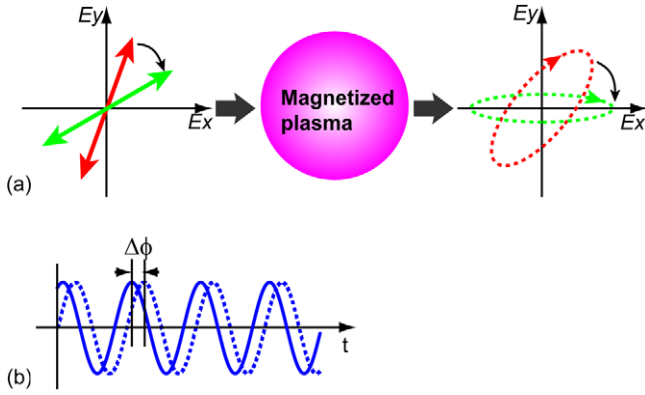


**Figure 2.** Schematic of the 288 GHz polarimeter. (a) A rotating linearly polarized microwave beam (solid) is launched into the magnetized plasma and the emerging polarizations (dashed) can be rotated and/or elliptized. (b) The signal sinusoidal waveform (dashed) is output by a polarization sensitive detector oriented in the toroidal direction and the reference sinusoidal waveform (solid) is generated during the process of producing the microwave. The phase shift between these two waveforms directly relates to the polarization change due to the magnetized plasma.

(FR, polarization rotation due to a magnetic field component parallel to the beam propagation) would advance the linear polarization rotation, resulting in a measured phase shift.

Polarimetry on NSTX poses challenges that are partly addressed by the choice of probing wavelength. The chosen millimeter ( $\lambda_0 = 1.04$  mm) wavelength is longer than common for polarimetry systems but is a good compromise between two competing constraints. On the one hand, at shorter wavelength, refraction becomes less significant, which is critical for the detector to efficiently receive the returning beam in this retroreflection geometry. On the other hand, at longer wavelengths the plasma effects on wave polarization are much stronger, potentially allowing for a more sensitive measurement of magnetic fluctuations, which is the primary motivation for the development of this polarimeter.

However, for millimeter-wave polarimetry on NSTX, the Cotton–Mouton (CM) effect (ellipticization due to magnetic field perpendicular to beam propagation) can be significant and can also interact with the FR effect [14, 15]. The CM effect has to be included when interpreting polarimetry measurements, especially in NSTX-U due to the somewhat larger toroidal field. A synthetic diagnostic code is developed for this purpose, which includes all magnetic field components and thereby includes both FR and CM effects as well as any interaction. Figure 3 shows an example of the impact of including the CM effect in calculating the predicted polarimetry phase response for the equilibrium plasma discussed. Calculated polarimeter phase versus chord height is compared using two different sets of assumptions for the calculation. The solid curve shows the case when the full calculations are performed, i.e. all components of the magnetic field are included; this includes both FR and CM effects as well as any interaction. In contrast, the dashed curve shows a calculation for the same plasma that only includes the horizontal component of the magnetic field, thereby including only the FR effect in isolation and suppressing the CM effect. The calculated

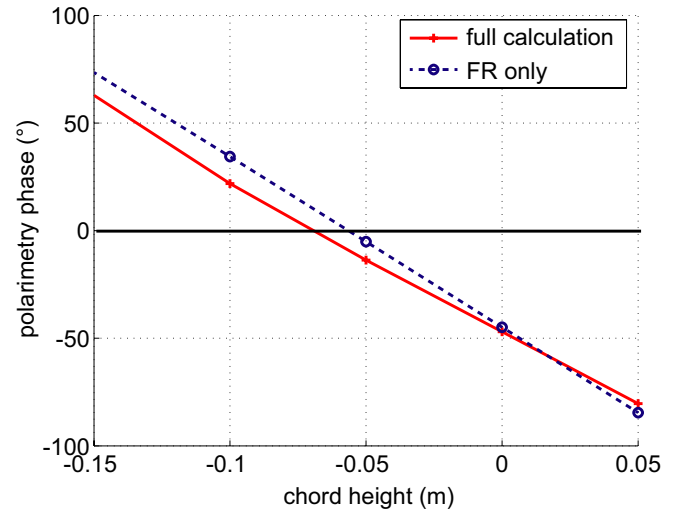


**Figure 3.** Synthetic height scan of the polarimeter viewing chord referenced to NSTX machine midplane. (shot #120968, time = 0.560 s, magnetic axis 5 cm below midplane) Polarimetry phases with a series of chord height are calculated by the synthetic diagnostic code. The solid curve shows the predicted phase with both Faraday rotation (FR) and Cotton–Mouton effects included. The dashed curve shows the predicted phase if only FR effect is included. A solid horizontal line highlights the zero phase.

phase is distinctly different for the two cases, indicating that experimental measurements would be misinterpreted if the measured phase were incorrectly assumed to be only caused by the FR effect. For instance, the zero phase point in the solid curve which would be observed at the height of the plasma magnetic axis (–5 cm) in the absence of the CM effect, is actually observed at –7 cm since the CM effect is significant (the ellipticity of the resultant polarization ellipse can be as large as 0.87). As described below, this synthetic diagnostic code is also a useful tool to assess the polarimeter sensitivity for measurement of magnetic fluctuations induced by microtearing modes, as well as coherent modes.

The code is a forward calculation code, using the Mueller–Stokes calculus to track the polarization evolution as the beam propagates [14, 16]. It calculates the Mueller matrices along the propagation and evaluates the resultant polarimetry phase shift at the detector. (Major steps are reviewed in the appendix.) It takes as the input of electron density and magnetic field along the diagnostic chord, and outputs predicted polarimetry phase. Using the time-varying density and magnetic profiles generated by the previously mentioned nonlinear gyrokinetic simulations, the code can calculate polarimetry phase at each instant of time, yielding a time-varying phase. It also provides an option to artificially suppress the FR and CM effects by suppressing individual components of the magnetic field, or density and magnetic fluctuations, to facilitate interpretation of the calculated polarimetry phase. The code assumes a beam propagation without refraction, which is a good assumption under most NSTX discharge conditions, where  $\omega_{pe}, \omega_{ce} \ll 288$  GHz. For the plasma equilibrium being discussed, beam refraction is estimated using a ray tracing code GENRAY [17], which calculates the beam trajectory inside the plasma. The returning beam at the plasma outboard

edge is predicted to vertically shift by only 2 cm, for a beam launched 0.2 m above the plasma midplane. This is the furthest away from the midplane that the diagnostic can operate, by vertically jogging the plasma across the fixed viewing chord. This prediction validates the ray tracing assumption since the estimated beam deflection is  $<0.4^\circ$ . The propagating beam has an approximately constant beam diameter of 5 cm, implying that the system is capable of detecting magnetic structures with  $k_\theta < 0.5 \text{ cm}^{-1}$  along the midplane [18], which is satisfactory for the study of microtearing modes.

### 3. Results and discussion

The polarimetry phase response to microtearing modes calculated by the synthetic diagnostic code is shown for several cases in figure 4. Figure 4(a) shows the case when a beam horizontally propagates through the plasma magnetic axis, which is 5 cm below the NSTX machine midplane for this plasma equilibrium; figure 4(b) shows the case when the diagnostic chord is 0.2 m above the machine midplane. The different curves in each panel correspond to cases where the radial magnetic and/or density fluctuations are artificially suppressed in the calculation. When all fluctuations are suppressed, only the plasma equilibrium information is utilized in the calculation. The black horizontal line (almost overlaid by the red in figure 4(a)) shows this situation in each panel, providing a reference phase with no fluctuations. The red curve, which shows only weak phase variation, corresponds to the case where the calculations include only the density fluctuations ( $\tilde{n}_e$ ). The blue curve includes both density and radial magnetic fluctuations ( $\tilde{n}_e + \tilde{B}_r$ ). The green curve, which is almost overlaid by the blue, includes only the radial magnetic fluctuations. As can be seen when both magnetic and density fluctuations are included, the code predicts  $\gtrsim 2^\circ$  peak-to-peak semi-coherent phase variation ( $f \sim 10 \text{ kHz}$ ). It is obvious from the similarity of the green and blue curves that the contribution to the blue curve is primarily from the magnetic fluctuations. The phase variations due to density fluctuations are negligible, when the beam propagates through the plasma magnetic axis, as illustrated in figure 4(a). This contribution becomes slightly more pronounced when the beam is farther away from the magnetic axis, as shown in figure 4(b), but is still relatively weak when compared with the phase variations induced by radial magnetic fluctuations alone. Other calculations for intermediate chord heights (not shown) are consistent with these conclusions. This is especially true for chord heights within  $\pm 5 \text{ cm}$  of the magnetic axis. The contribution of perpendicular in-flux-surface, or binormal, magnetic fluctuations ( $\tilde{B}_\theta$ ) is neglected. The maximum possible contribution from this component is assessed by a worst case calculation, which assumes a perturbation with a uniform profile and a magnitude equal to the maximum of the radial component, i.e.  $30 \text{ G}$ . This is an upper-limit for the neglected component since  $\tilde{B}_\theta \sim k_r \tilde{A}$ , while  $\tilde{B}_r \sim k_\theta \tilde{A}$ , and it can be seen, by inspection of figure 2(b) in [1], that  $|k_r \tilde{A}| < |k_\theta \tilde{A}|$ , for the gyrokinetic simulation results considered. This calculation suggests the contribution is  $<10\%$  of the total phase fluctuations, so the following discussions of magnetic

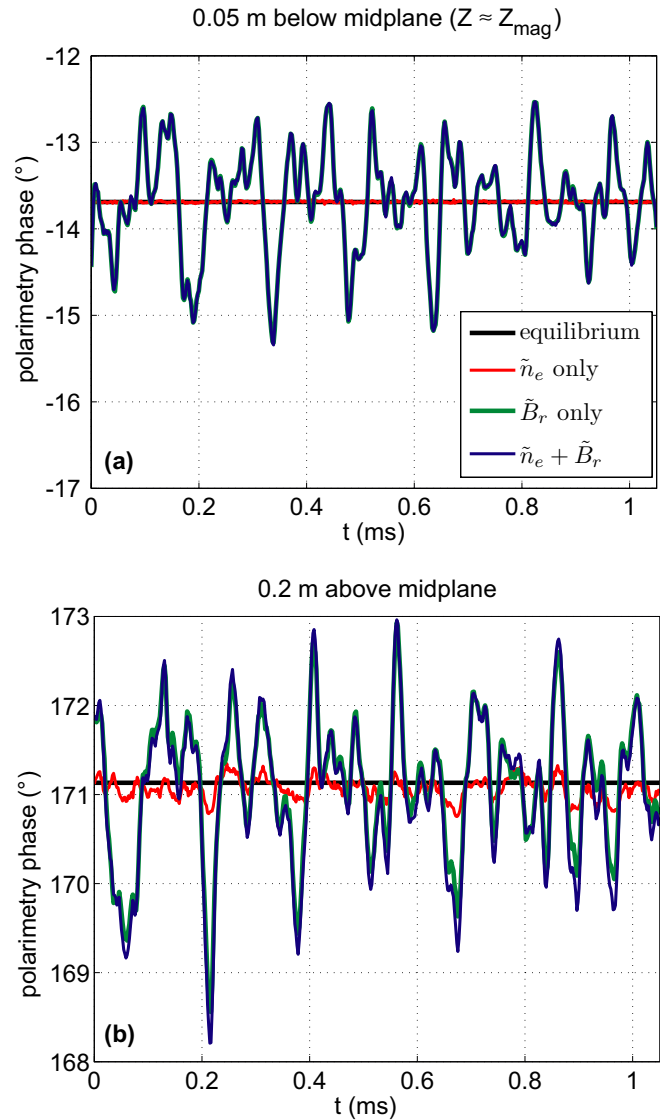


**Figure 4.** Polarimetry phase calculated by the synthetic diagnostic code using fluctuation profiles generated by nonlinear gyrokinetic simulations for a beam horizontally propagating across the plasma magnetic axis (a), and 0.2 m above the machine midplane (b). Black horizontal line shows the equilibrium phase; red curve shows the fluctuating phase with only density fluctuations ( $\tilde{n}_e$ ) included; green curve includes only radial magnetic fluctuations ( $\tilde{B}_r$ ); blue curve includes both density and magnetic fluctuations ( $\tilde{n}_e + \tilde{B}_r$ ). Also note the blue curve almost overlays the green curve and the red curve only shows very weak variations around the black horizontal line.

fluctuations refer only to the radial component. A more comprehensive consideration will be the subject of future work.

The approximately 10 kHz phase fluctuations visible in the calculations shown in figure 4 are predicted to be detectable since their level is above the measured phase resolution of the polarimeter, which is  $\sim 0.3^\circ$  in a frequency range  $1 \text{ kHz} < f < 100 \text{ kHz}$ . Note that the gyrokinetic simulation results considered here do not include plasma rotation ( $\sim 10 \text{ kHz}$  typical). Considering that the microtearing modes have large  $n$  numbers ( $n = 5$  is shown in figure 1(a)), the fluctuation frequency observed in an experiment will be substantially Doppler shifted but still in the range of sensitivity. The

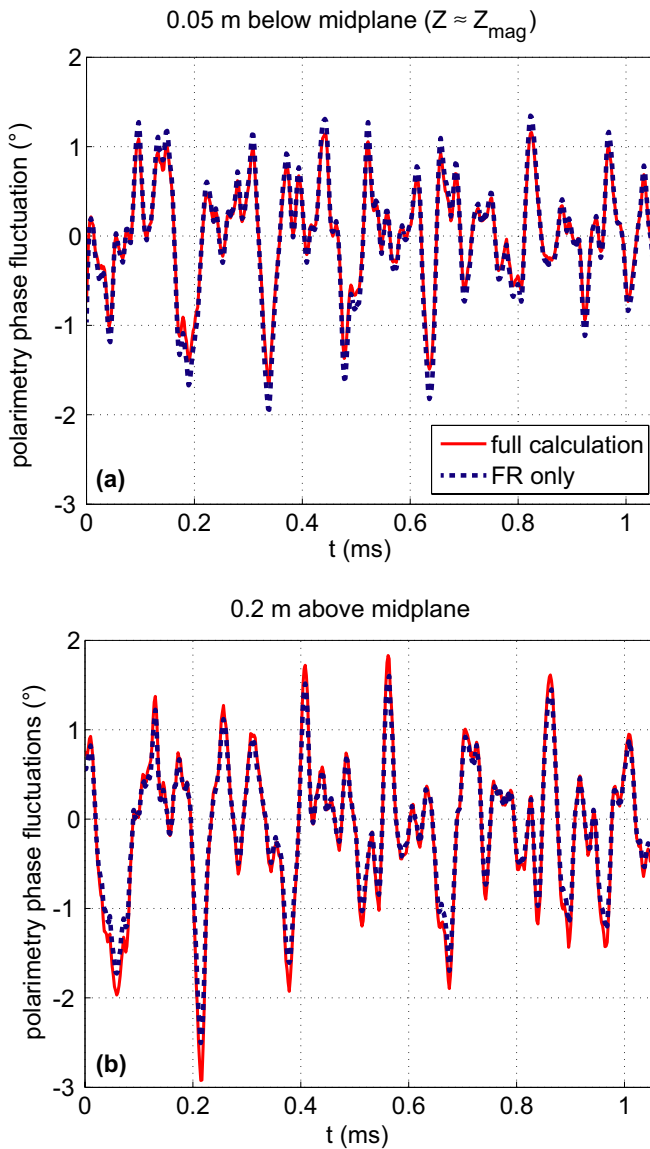


**Figure 5.** Polarimetry phase fluctuations calculated by the synthetic diagnostic code for the chord across the plasma magnetic axis (a) and 0.2 m above the machine midplane (b). The solid curve shows the phase fluctuations with both Faraday rotation (FR) and Cotton–Mouton effects included. The dashed curve shows the results including only the FR effect.

sensitivity of the polarimetry phase primarily to the FR effect caused by magnetic fluctuations results from two facts. First, of the various magnetic field effects that can contribute to the polarimeter phase fluctuation ( $\tilde{\phi}$ ), the dominant contribution is from the FR ( $\tilde{\psi}$ ) effect. Figure 5 illustrates that including the CM effect from the equilibrium magnetic field makes little difference to the calculated phase fluctuations for the same chord heights shown in figure 4. Also, as noted above, the CM effect from  $\tilde{B}_\theta$  is expected to be small. Second, the geometry of the diagnostic minimizes the contribution of density fluctuations to the FR effect. Due to the relatively minor contribution from the CM effect, the resultant fluctuating phase can then be represented to first order by

$$\tilde{\phi} \approx 2\tilde{\psi} \xrightarrow{\text{to 1st order}} C \int \tilde{n}_e \tilde{B}_\parallel dl + C \int \tilde{n}_e \tilde{B}_\parallel dl, \quad (1)$$

where  $C$  is a constant factor for a fixed wavelength,  $B_\parallel$  is the magnetic field component parallel to the beam propagation, which is along the major radius in this case, and ‘ $-$ ’ and ‘ $\sim$ ’ represent equilibrium and fluctuation quantities, respectively [8]. Since propagation close to the plasma midplane means that the equilibrium  $B_\parallel$  is always close to zero, the density fluctuation contribution to equation (1) is much smaller than that due to magnetic fluctuations. However, as the chord moves away from the midplane, density fluctuations start to contribute (see figure 4) due to the increasing equilibrium  $B_\parallel$ .

#### 4. Conclusion

This paper has investigated the possibility of measuring magnetic fluctuations associated with microtearing modes in NSTX-U using a planned 288 GHz polarimeter. A synthetic diagnostic code developed for the polarimeter was employed to calculate the polarimetry phase response to input density and magnetic fluctuation profiles. The output fluctuation profiles ( $\tilde{n}_e$  and  $\tilde{B}_r$ ) predicted from nonlinear gyrokinetic simulations of microtearing modes in NSTX were used as input to the synthetic phase calculations. The results indicate that the phase fluctuations resulting from the simulated microtearing modes have a fluctuation frequency centered around 10 kHz and fluctuation level of  $\gtrsim 2^\circ$ , which is detectable. The phase fluctuations measured near the plasma midplane (within  $\pm 5$  cm) are found to be dominated by the magnetic, not density fluctuations. This result is due to two facts: the fluctuations from FR contribute to the final phase fluctuations substantially more than the CM effect, and the equilibrium magnetic field is almost perpendicular to the probing chord near plasma midplane, so that the fluctuating parallel magnetic field dominates the resultant phase fluctuations. From the above it is concluded that the proposed polarimeter should have sufficient sensitivity to observe magnetic fluctuations associated with microtearing modes in NSTX-U.

#### Appendix. Mueller–Stokes calculus [14, 16]

The polarization of an electromagnetic (EM) wave can be represented by a Stokes vector,  $\vec{s}_{4 \times 1}$ . As the EM wave propagates through a magnetized plasma ( $\omega \gg \omega_{pe}$ ,  $\omega_{ce} \gg \omega_{pi}$ ,  $\omega_{ci}$ , where  $\omega$  is the angular frequency of the EM wave,  $\omega_p = \sqrt{nq^2/m\epsilon_0}$ ,  $\omega_c = |q|B/m$ , and subscripts ‘i’ and ‘e’ stand for ions and electrons, respectively), its polarization evolves following the equation:  $\vec{s}(z)_{4 \times 1} = M(z)_{4 \times 4} \cdot \vec{s}(0)_{4 \times 1}$ , where  $z$  is the path parameter along the propagation and  $M$  is the Mueller matrix. With the knowledge of Mueller matrices along the path, the polarization evolution of any EM wave can be fully characterized.

Several assumptions can be made to further simplify the Mueller–Stokes analysis. The plasma is assumed to be collisionless, so the beam experiences no dissipation. A cold plasma model is adopted, which excludes corrections from finite temperature effects. The Wentzel–Kramers–Brillouin approximation is used, i.e. plasma parameters are assumed to be slowly varying ( $|\vec{B}| \gg |(1/k)(\partial \vec{B}/\partial z)|$ ,  $|n| \gg |(1/k)(\partial n/\partial z)|$ ).

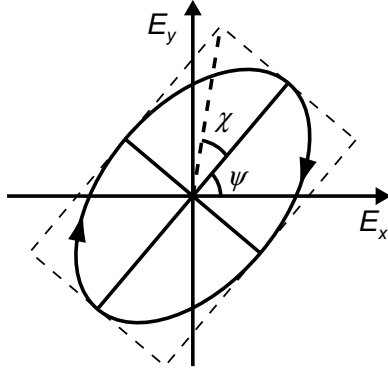


**Figure A1.**  $E$ -field ellipse of a polarized EM wave. It can be characterized by two parameters, elliptization angle  $\chi$  and polarization direction angle  $\psi$ .

With these assumptions, the Stokes vector can be reduced to a  $3 \times 1$  vector:

$$\vec{s}_{3 \times 1} = \begin{pmatrix} s_1 \\ s_2 \\ s_3 \end{pmatrix} = \begin{pmatrix} \cos 2\chi \cos 2\psi \\ \cos 2\chi \sin 2\psi \\ \sin 2\chi \end{pmatrix},$$

where  $\chi$  and  $\psi$  are the two parameters characterizing the  $E$ -field ellipse of the polarized EM wave (figure A1); the Mueller matrix is also reduced to  $3 \times 3$  dimension:

$$M = \begin{pmatrix} M_{11} & M_{12} & M_{13} \\ M_{21} & M_{22} & M_{23} \\ M_{31} & M_{32} & M_{33} \end{pmatrix}.$$

In differential form the evolution of a Stokes vector also obeys

$$\frac{d\vec{s}(z)}{dz} = \vec{\Omega}(z) \times \vec{s}(z), \quad (\text{A1})$$

in which  $\vec{\Omega}$  is defined by local plasma parameters:

$$\vec{\Omega} = \frac{\omega_{pe}^2 \omega_{ce}^2}{2c\omega(\omega^2 - \omega_{ce}^2)} \begin{pmatrix} (B_x^2 - B_y^2)/B^2 \\ 2B_x B_y/B^2 \\ 2(\omega/\omega_{ce})B_z/B \end{pmatrix}, \quad (\text{A2})$$

where the  $xyz$  coordinate system is defined in the EM wave frame.

The synthetic diagnostic code utilized in this work traces the Stokes vector evolution using equation (A1), with three mutually orthogonal input boundary conditions:

$$\vec{s}(0) = \begin{pmatrix} 1 \\ 0 \\ 0 \end{pmatrix}, \begin{pmatrix} 0 \\ 1 \\ 0 \end{pmatrix}, \begin{pmatrix} 0 \\ 0 \\ 1 \end{pmatrix},$$

and correspondingly the output Stokes vectors are

$$\vec{s}(z) = \begin{pmatrix} M_{11}(z) \\ M_{21}(z) \\ M_{31}(z) \end{pmatrix}, \begin{pmatrix} M_{12}(z) \\ M_{22}(z) \\ M_{32}(z) \end{pmatrix}, \begin{pmatrix} M_{13}(z) \\ M_{23}(z) \\ M_{33}(z) \end{pmatrix}.$$

By properly arranging the output Stokes vector elements, the  $3 \times 3$  Mueller matrices are acquired along the wave path.

For the polarimeter system described in this paper, the input boundary condition (linear polarization rotates at frequency of  $\varpi/2$ ) is

$$\vec{s}(0) = \begin{pmatrix} \cos \varpi t \\ \sin \varpi t \\ 0 \end{pmatrix},$$

and the resultant Stokes vector can be calculated from the previously acquired Mueller matrices:

$$\vec{s}(z) = \begin{pmatrix} M_{11}(z) \cos \varpi t + M_{12}(z) \sin \varpi t \\ M_{21}(z) \cos \varpi t + M_{22}(z) \sin \varpi t \\ M_{31}(z) \cos \varpi t + M_{32}(z) \sin \varpi t \end{pmatrix}.$$

For a detector oriented to detect  $|E_x|^2$  of the output wave ( $z = 2L$ ), it will output a sinusoidal wave with the polarimetry phase shift:

$$\phi = \tan^{-1} \left( \frac{M_{11}(2L)}{M_{12}(2L)} \right).$$

## References

- [1] Guttenfelder W *et al* 2011 *Phys. Rev. Lett.* **106** 155004
- [2] Zhang J *et al* 2012 *Rev. Sci. Instrum.* **83** 10E321
- [3] Menard J E *et al* 2012 *Nucl. Fusion* **52** 083015
- [4] Dodel G and Kunz W 1978 *Infrared Phys.* **18** 773
- [5] Braithwaite G, Gottardi N, Magyar G, O'Rourke J, Ryan J and Veron D 1989 *Rev. Sci. Instrum.* **60** 2825
- [6] Fuchs Ch and Hartfuss H J 1998 *Phys. Rev. Lett.* **81** 1626
- [7] Koslowski H R, Soltwisch H and Stodiek W 1996 *Plasma Phys. Control. Fusion* **38** 271
- [8] Ding W X, Brower D L, Terry S D, Craig D, Prager S C, Sarff J S and Wright J C 2003 *Phys. Rev. Lett.* **90** 035002
- [9] Drake J F and Lee Y C 1977 *Phys. Fluids* **20** 1341
- [10] Levinton F M *et al* 2007 *Phys. Plasmas* **14** 056119
- [11] Applegate D J *et al* 2007 *Plasma Phys. Control. Fusion* **49** 1113
- [12] Wong K L *et al* 2007 *Phys. Rev. Lett.* **99** 135003
- [13] Guttenfelder W *et al* 2012 *Phys. Plasmas* **19** 056119
- [14] Zhang J, Crocker N A, Carter T A, Kubota S and Peebles W A 2010 *Rev. Sci. Instrum.* **81** 10D519
- [15] Orsitto F P *et al* 2010 *Rev. Sci. Instrum.* **81** 10D533
- [16] Segre S E 1999 *Plasma Phys. Control. Fusion* **41** R57
- [17] Smirnov A P and Harvey R W 1995 *Bull. Am. Phys. Soc.* **40** 1837
- [18] Jiang Y, Brower D L and Lanier N E 1999 *Rev. Sci. Instrum.* **70** 703